

AperTO - Archivio Istituzionale Open Access dell'Università di Torino

Mapping post-fire monthly erosion rates at the catchment scale using empirical models implemented in GIS. A case study in Northern Italy

This is a pre print version of the following article:

Original Citation:

Availability:

This version is available <http://hdl.handle.net/2318/1880239> since 2022-11-24T11:31:07Z

Publisher:

Springer

Terms of use:

Open Access

Anyone can freely access the full text of works made available as "Open Access". Works made available under a Creative Commons license can be used according to the terms and conditions of said license. Use of all other works requires consent of the right holder (author or publisher) if not exempted from copyright protection by the applicable law.

(Article begins on next page)

Metadata of the chapter that will be visualized in SpringerLink

Book Title	Progress in Landslide Research and Technology, Volume 1 Issue 1, 2022	
Series Title		
Chapter Title	Mapping Post-fire Monthly Erosion Rates at the Catchment Scale Using Empirical Models Implemented in GIS. A Case Study in Northern Italy	
Copyright Year	2023	
Copyright HolderName	The Author(s)	
Author	Family Name	Vacha
	Particle	
	Given Name	Damiano
	Prefix	
	Suffix	
	Role	
	Division	Interuniversity Department of Regional and Urban Studies and Planning (DIST)
	Organization	University of Turin
	Address	10125, Turin, Italy
	Email	damiano.vacha@unito.it
Corresponding Author	Family Name	Mandrone
	Particle	
	Given Name	Giuseppe
	Prefix	
	Suffix	
	Role	
	Division	Interuniversity Department of Regional and Urban Studies and Planning (DIST)
	Organization	University of Turin
	Address	10125, Turin, Italy
	Email	giuseppe.mandrone@unito.it
Author	Family Name	Morresi
	Particle	
	Given Name	Donato
	Prefix	
	Suffix	
	Role	
	Division	Department of Agricultural, Forest and Food Sciences (DISAFA)
	Organization	University of Turin
	Address	10095, Grugliasco, TO, Italy
	Email	donato.morresi@unito.it
Author	Family Name	Garbarino
	Particle	
	Given Name	Matteo

Prefix
Suffix
Role
Division Department of Agricultural, Forest and Food Sciences (DISAFA)
Organization University of Turin
Address 10095, Grugliasco, TO, Italy
Email matteo.garbarino@unito.it

Abstract Post-wildfire geological hazards are an emerging problem for a number of different environments, including areas not typically associated with these events such as the Alpine Region. The risk connected with post-fire processes such as debris-flows and flood-type events threatens people, infrastructures, services and economical activities. Apart from a few examples, such as in the USA and Australia, there is a lack of models available to quantify the increase in susceptibility of the aforementioned phenomena as a result of the modification induced by the wildfires. In this work we test the application of a modified version of the RUSLE, on GIS, to quantify the post-fire erosive phenomena for a case study in the north-western Italian Alps. The results of its application, taking advantage of high-resolution rainfall series and data deriving from field surveys, highlight the marked increase (more than 20 times) in erosion rates, quantified by expressing both the EI (erodibility index), the A (monthly soil loss) and the SL (monthly sediment loss) rise. The months of April, May and June represent the larger share of the total quantities. This is a consequence of the noticeable increase of the EI, which for the post-fire scenario is more than one order of magnitude higher than the pre-fire one.

Keywords Wildfires - Erosion - Slope stability - Hazard - Western Alps
(separated by '-')



Author Proof

Mapping Post-fire Monthly Erosion Rates at the Catchment Scale Using Empirical Models Implemented in GIS. A Case Study in Northern Italy

Damiano Vacha, Giuseppe Mandrone, Donato Morresi, and Matteo Garbarino

Abstract

Post-wildfire geological hazards are an emerging problem for a number of different environments, including areas not typically associated with these events such as the Alpine Region. The risk connected with post-fire processes such as debris-flows and flood-type events threatens people, infrastructures, services and economical activities. Apart from a few examples, such as in the USA and Australia, there is a lack of models available to quantify the increase in susceptibility of the aforementioned phenomena as a result of the modification induced by the wildfires. In this work we test the application of a modified version of the RUSLE, on GIS, to quantify the post-fire erosive phenomena for a case study in the north-western Italian Alps. The results of its application, taking advantage of high-resolution rainfall series and data deriving from field surveys, highlight the marked increase (more than 20 times) in erosion rates, quantified by expressing both the EI (erodibility index), the A (monthly soil loss) and the SL (monthly sediment loss) rise. The months of April, May and June represent the larger share of the total quantities. This is a consequence of the noticeable increase of the EI, which for the post-fire scenario is more than one order of magnitude higher than the pre-fire one.

Keywords

Wildfires • Erosion • Slope stability • Hazard • Western Alps

1 Introduction

Climate change is having far-reaching effects ranging from unprecedented forest fires, heatwaves, droughts and extreme rainfall events (IPCC 2014a, b). Natural disturbances are thought to experience a further increase in frequency and severity, progressively affecting areas not endangered in the past also due to land use change (Maringer et al. 2016; Mantero et al. 2020). They can occur alone or in combination with each other and cause and/or be followed by secondary hazards, constituting a complex chain of multi-hazards processes also called cascading effect. As an example, forest fires lead to new avalanche-prone slopes, and to a higher risk of rockfall, debris-flow, mudslides, soil erosion and water quality problems. Recent estimates for the Alpine region, forecasting an increased impact of the climate change effects, suggest wildfires and post-wildfire geological hazards to represent a looming issue in the near future (Zumbrunnen et al. 2009; Moreira et al. 2011; Wastl et al. 2012; Arndt et al. 2013, Dupire et al. 2019, Barbero et al. 2019).

Amongst other hydrological hazards, debris-flow and flood-type events represent the most serious concern, as can be seen in the reports and the scientific literature of the regions (USA, Australia) which are facing the problem nowadays (De Graff 2014). The modification of the hydrological properties, due to litter and vegetation removal, ash deposition, alteration of the physical properties of soil and rocks results in an increase of the availability of easily erodible materials on hillslopes and of runoff rates (Moody and Martin 2001; Parise and Cannon 2008, 2012; Staley et al 2017). In fact, rainsplash, sheetflow and rill erosion

D. Vacha · G. Mandrone (✉)
Interuniversity Department of Regional and Urban Studies and Planning (DIST), University of Turin, 10125 Turin, Italy
e-mail: giuseppe.mandrone@unito.it

D. Vacha
e-mail: damiano.vacha@unito.it

D. Morresi · M. Garbarino
Department of Agricultural, Forest and Food Sciences (DISAFA), University of Turin, 10095 Grugliasco, TO, Italy
e-mail: donato.morresi@unito.it

M. Garbarino
e-mail: matteo.garbarino@unito.it



increases due to the diminished capacity of rainfall interception by the tree canopies, shrubs and grass. Very soon the surface runoff may concentrate in hollows and low order channels carrying the eroded sediment and entraining the materials deposited in the waterways, eventually exerting a strong erosive action at the expense of the riverbed sediments and causing their “in mass” failure. All of these processes can lead to sediment concentration to levels associated with debris flows (Thang et al. 2019).

Currently, very few models are available for the estimate of the hazard and risk of these phenomena. The USGS preliminary hazard assessment relies on empirical models to assess the likelihood, volume and combined hazard of debris flows for selected watersheds in response to a design storm. These models rely on historical debris–flow occurrence and magnitude data, rainfall storm conditions, terrain and soils information, and burn–severity maps (Staley et al. 2016, 2017). In Australia, the Victorian Department of Sustainability and Environment (DSE) developed an empirical rapid risk assessment procedure for post-fire hydrologic risks, namely debris flows risk, water quality risk and flooding risk. The model, in the early stages of development, is based on available datasets and combines information for terrain, vegetation, rainfall erosivity, burn severity maps and stream network (Sheridan et al. 2009). In other countries, such as the Mediterranean ones, despite an increasing number of hazardous events (Parise and Cannon 2008; Tiranti et al. 2006; Carabella et al. 2019; Esposito et al. 2013, 2017, 2019), no model for the hydro-geomorphic events susceptibility assessment has been implemented or validated extensively. Very few examples of model application can be found in Italy, Greece, Portugal and Spain (Terranova et al. 2009; Fernandez et al. 2010, 2018; Coschignano et al. 2019; Esteves et al. 2013; Rulli et al. 2013; Lanorte et al. 2019; Depountis 2020, Efthimiou 2020). The need to quantify the influence of fires on the propensity for hazardous processes clashes with the fact that, in many regions outside the United States, the scientific community has faced the problem in a consistent way only in recent years and thus the available post-fire event statistics does not allow for a data driven approach. In this study, we focused on the application and validation of a modified version of the RUSLE model (Revised Universal Soil Loss Equation—Wischmeier and Smith 1978) to quantify the post-fire erosive phenomena for a case study in the north-western Italian Alps. In this area, during October 2017, ten wildfires occurred, burning a total area of 10,000 hectares of which 7000 were forests; this value far exceeds the average regional forest burned area (600 ha/year between 2005 and 2013) (Morresi et al. 2022). Season fires in 2017 were favored by the exceptionally dry conditions, high temperatures and the occurrence of several days with hot and dry winds (Arpa Piemonte 2017; Bo et al. 2020). The largest and most severe fire—almost 4000 ha—

occurred in the Susa Valley, where fourteen catchments on the left of the Dora Riparia River were involved. Starting from late April 2018 until the early June, several flow events originated from the burned catchments. The larger damages were recorded at the outlet of the Comba delle Foglie, a small drainage basin overhanging the Bussoleno municipality (Vacha et al. 2021). Ground evidence highlighted a remarkable increase in erosion rates exerted by the surface runoff in many sectors within the fire perimeter, in agreement with literature findings (Moody and Martin 2001; Parise and Cannon 2008, 2012; Staley et al. 2017). Based on the assumption that these processes represent the key aspect governing the availability of sediments to be entrained during rainfalls, and taking into account the available spatial data, the structure of the RUSLE model proved to be the most suitable framework to be adopted. In fact, the approach used is deliberately simple, replicable, improvable and easy to implement in a GIS environment. It is also possible to automate it in order to make it available for the rapid production of thematic maps to support authorities and for civil protection purposes. Moreover, it relies mostly on the available open source spatialized data provided by regional authorities and other public bodies, which makes it easy to replicate the conceptual scheme in other areas. The model has been applied and validated on the Comba delle Foglie catchment, for which a detailed temporal reconstruction of the processes and quantification of the volume of mobilized material has been carried out in a previous work (Vacha et al. 2021).

2 Study Area

The study area is located in the Susa Valley, an east–west Alpine valley, located in the western part of Piedmont (starting ~ 20 km West of Turin). It was affected by the largest and more severe of the ten wildfires that occurred in the region in 2017 (The Bussoleno and Mompantero Wildfire) which burned 4000 ha on the left of the Dora Riparia River, going up the valley from east to west and affecting the slope almost to the divide (Fig. 1). The fire started on October 22, 2017 and lasted until November 1, 2017. It interested an area dominated by European Beech (*Fagus sylvatica* L.) and Scots Pine (*Pinus sylvestris* L.), the forest cover being the 37.1% and the 26.7% for the Broadleaved and the Coniferous species, respectively, with 36.2% of the wildfire surface being represented by non-forested areas (Morresi et al. 2022). Comba delle Foglie is one of the catchments affected by this exceptional wildfire. It is located towards the eastern side of the wildfire area and is a steep, elongated watershed ranging between 480 and 1747 m a.s.l., characterized by an average slope of 35° and an area of approximately 1.37 km² (Vacha et al. 2021). The bedrock

of the catchment is represented by polymetamorphic rocks and in particular by Micaschists and gneiss belonging to the Dora Maira pre-triassic basement (DMb), by calcschists, marbles and dolomitic marbles belonging to the Dora Maira Mesozoic cover (DMc) and by calcschists, serpentinites, serpentinoschists and chloritoschist belonging to the Lower Piedmont Zone (PZ) (Carraro et al. 2002; Gasco et al. 2011). The geomorphological setting of the study is both influenced by its geologic history and by quaternary geomorphic events. The main valley is dominated by erosional and depositional landforms of glacial origin, mainly glacial terraces, suspended-tributary valleys and lodgement and ablation till. The post-glacial remodeling action exerted by gravitative and fluvial processes strongly influenced the landscape. In particular, the left side of the Susa Valley hosts a series of ravine and canyon-like features in correspondence of morphological steps at the outlet of suspended valleys into the main valley. As a result, the quaternary deposits mantle the study area heterogeneously: the main valley floor is filled by alluvial deposits, while the slope are patched by glacial, fluvial and gravity related deposits, often reworked (Cadoppi et al. 2007).

The vegetative cover of the catchment before the fire was low with respect to other sectors of the burned area due to previous wildfires (Ascoli et al. 2011), and it was mostly dominated by young trees of *Populus tremula* and *Salix caprea*. The most relevant parameters describing the watershed are given in Table 1, in which the major morphometric descriptors can be found.

3 Materials and Methods

3.1 Burn Severity

The burn severity map of the Bussoleno and Mompantero Wildfire (Morresi et al. 2022) was adopted in this work. This map was produced through satellite imagery and field surveys, following a methodology based on US FIREMON framework (Key and Benson 2005). The analysis of spectral changes caused by the 2017 wildfires was carried out using multispectral images acquired by the MultiSpectral Instrument (MSI) onboard Sentinel-2 A/B satellites (European Space Agency). In particular, the burn severity obtained by using the uncalibrated RdNBR bi-temporal index (Miller and Thode 2007, Eq. 1) calculated from reflectance composites was adopted here. It was generated using all the clear observations available in the period spanning from 20 May to 10 September for both 2017 and 2018; the validation of the map and the classification in severity categories followed Miller et al. (2009), Miller and Thode (2007) and Parks et al. (2014). This product was chosen because among all the other indices calculated by the authors, it was the one with the best overall accuracy.

$$RdNBR = \frac{dNBR}{\sqrt{|NBR_{prefire}|}} \quad (1)$$

RdNBR is based on the definition of the Normalized Burn Ratio (NBR) (Eq. 2) which is calculated by contrasting the

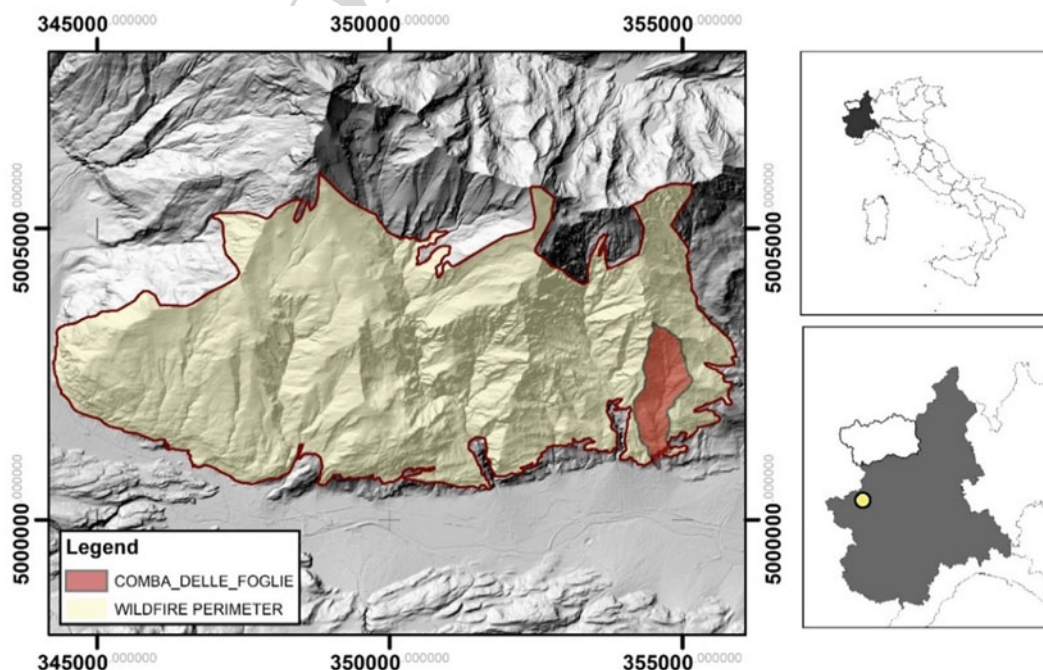


Fig. 1 Perimeter of the Susa valley wildfire and location of the Comba delle Foglie watershed. The base map is the regional DTM

Table 1 Morphometrical and hydrological descriptors of the Comba delle Foglie watershed; area A_w [km^2], perimeter P [km], watershed length L_b [km], minimum elevation E_{min} [m s.l.m.], maximum elevation E_{max} [m s.l.m.], mean elevation E_{mean} [m s.l.m.], minimum slope S_{min} [$^\circ$], maximum slope S_{max} [$^\circ$], mean slope S_{mean} [$^\circ$], main channel length L_p [km], average main channel slope L_pS [$^\circ$], total streams length L [km], Fan to watershed area ratio A_f/A_w [-], Form factor F_f [-] (Horton 1932), Circularity ratio R_c [-] (Miller 1953; Strahler 1964), Elongation ratio R_e [-] (Schumm 1956), Melton Index M_e [-] (Melton 1965), Drainage density D_d [km/km^2] (Strahler 1964), Time of concentration T_c [h] (Kirpich 1940)

Index	Unit	Value	Index	Unit	Value	Index	Unit	Value
A_w	[km^2]	1.37	S_{max}	[$^\circ$]	74.82	A_f/A_w	[-]	8.14
P	[km]	6.1	S_{mean}	[$^\circ$]	35.01	F_f	[-]	0.22
L_b	[km]	2.59	L_p	[km]	2.44	R_c	[-]	0.44
E_{min}	[m a.s.l.]	480	L_pS	[$^\circ$]	32.22	R_e	[-]	0.53
E_{max}	[m a.s.l.]	1747	L	[km]	4.14	M_e	[-]	1.02
E_{mean}	[m a.s.l.]	1035				D_d	[km/km^2]	3.19
S_{min}	[$^\circ$]	1.5				T_c	[h]	0.18

reflectance in the near infrared (NIR) and in the shortwave infrared (SWIR); the delta Normalized Burn Ratio (Key and Benson 2006) is calculated through Eq. (3).

$$NBR = [(NIR - SWIR)/(NIR + SWIR)] \quad (2)$$

$$dNBR = (NBR_{\text{prefire}} - NBR_{\text{postfire}}) \times 1000 \quad (3)$$

RUSLE—Monthly erosion calculation

Sediment erosion has been assessed implementing the RUSLE model at a monthly scale through the following equation:

$$A_{\text{month}} = R_{\text{month}} * K * L * S * C * P \quad (4)$$

where A = mean soil loss per month [$\text{Mg ha}^{-1} \text{m}^{-1}$], R = rainfall erosivity factor [$\text{MJ mm h}^{-1} \text{ha}^{-1} \text{m}^{-1}$], K = soil erodibility factor [$\text{Mg MJ}^{-1} \text{mm}^{-1} \text{h}$], L = topographic factor or slope length factor [dimensionless], C = soil coverage [dimensionless], and P = erosion control practices factor [dimensionless]. The value of the sediment loss (SL) is obtained by multiplying the value of A for the drainage surface. The R factor quantifies the mechanical impact energy exerted by a given precipitation and depends on duration and intensity of the rainfall. Remaining parameters in the equation give a measure of the environmental resistance to erosive phenomena. The K , L and C factors are assumed to change in areas affected by wildfires as a result of fire effect on soil erodibility, vegetative cover and shift in rill to interrill soil erodibility ratio (Terranova et al. 2009). RUSLE model is intended to quantify soil losses in the long term, so that processes such as gully and channel erosion and sediment transport cannot be modelled. Prediction accuracy for individual storm is very low, as controversial is the application on large spatial scale. Despite this,

the model can be used as a solid framework to quantify high-risk erodible areas (Efthimiou et al. 2020). With this regard, the product of K , L and C factor is used to compare post-fire to pre-fire condition; thus, EI [$\text{Mg MJ}^{-1} \text{mm}^{-1} \text{h}$] is introduced to describe the erosion susceptibility:

$$EI = C * K * L * S \quad (5)$$

P factor has been considered equal to 1, because there are no support practices for the erosion reduction in the study area.

Rainfall erosivity factor— R

The rainfall erosivity factor (R) factor has been estimated at a monthly scale by calculating the summation of the parameter EI_{30} of every single erosive event (k) for each considered month.

$$R_{\text{month}} = \sum_{k=1}^n EI_{30k} \quad (6)$$

Following Brown and Foster (1987), EI_{30} for a single rainstorm event is defined as the product of the kinetic energy of rainfall events (E) and its maximum 30-min intensity (I_{30}):

$$EI_{30} = \left(\sum_{r=1}^m e_r v_r \right) I_{30} \quad (7)$$

where e_r = unit rainfall energy [$\text{MJ ha}^{-1} \text{mm}^{-1}$], v_r = rainfall volume [mm] during the r -th period of a storm which divided into m parts and I_{30} is the maximum 30-min rainfall intensity [mm h^{-1}]. The unit rainfall energy e_r is calculated for each time interval using Eq. (8) (Brown and Foster, 1987):

$$e_r = 0.29 \left[1 - 0.72e^{(-0.05i_r)} \right] \quad (8)$$

Table 2 Location of the three rain gauges of Prarotto, Borgone and Malciaussia

Name	Elevation (m s.l.m.)	WGS84-UTM32N X (m)	WGS84-UTM32N Y (m)	Basin
Prarotto	1440	361,493	5,000,737	Dora riparia
Borgone	400	361,958	4,997,582	Dora riparia
Malciaussia	1800	354,590	5,007,700	Stura di lanzo

where i_r is the rainfall intensity during the time interval [mm h⁻¹]. High resolution rainfall data (10 min time resolution) were downloaded from Arpa Piemonte database for three rain gauges located in the surrounding of the watershed, namely Prarotto, Borgone and Malciaussia (Table 2 and Fig. 2). Rainfall series covers a period of time ranging from September 1, 2017 to August 3, 2018. The identification of the erosive rainfall (n) events for each station record followed three criteria given by Renard et al. (1997): the cumulative rainfall of an event is greater than 12.7 mm, or the event has at least one peak that is greater than 6.35 mm during a period of 15 min. Individual storms are separated if a rainfall accumulation is less than 1.27 mm during a period of 6 h. Those criteria have been developed for the USA countries, but are also widely accepted in other areas (Panagos et al. 2015a). The Rainfall Intensity Summarisation Tool (RIST) software (USDA 2014) was used to calculate the R-factor based on the single station annual series. After that, the single monthly R factors related to each rain gauge were averaged to get the final value representative of the watershed. The obtained results were compared with the average monthly rainfall erosivity calculated by Ballabio et al. (2017) at European scale analyzing > 17 years of rainfall data and downloaded from ESDAC repository (European Soil Data Centre, European Commission, Joint Research Centre).

Soil erodibility factor—K

The soil erodibility (K) factor has been determined based on soil textural data. Homogeneous lithological units have been individuated by grouping the geological units derived from 1:50,000 geological map (Carraro et al. 2002). Soil samples have been then collected and processed in laboratory for determining grain size distribution following standard ASTM procedures. Afterwards, the K factor for each unit has been then calculated based on the following formulae (Renard et al. 1997):

$$K = 0.0034 + 0.0405 * \exp \left[-0.5 \left(\frac{\log D_g + 1.659}{0.7101} \right)^2 \right] \quad (9)$$

$$D_g = \exp \left[\sum f_i \ln \left(\frac{d_i + d_{i-1}}{2} \right) \right] \quad (10)$$

where D_g = geometric mean particle size for each particle size class (clay, silt, sand), d_i = maximum diameter (mm), d_{i-1} = minimum diameter and f_i is the corresponding mass fraction.

Cover factor—C

The C factor has been assessed based on Forestry/Land Cover Map and by assigning C values according to Panagos et al. (2015b). Tabulated values for each land cover class are given in Table 3, whilst land cover classes areal distribution is given in Table 4.

Length/Slope Factor LS

The LS factor in the original RUSLE model describes the interaction between standard parcel length (L) and slope (S). In this study, it is substituted by the unit contributing area L_s , which takes into account the flow convergence (Mitasova et al. 1996; Terranova et al. 2009). L_s is computed for each 5 m wide DTM cell as follows:

$$L_s = (\mu + 1)(a/a_0)^\mu (\sin b/b_0)^\eta \quad (11)$$

where a [m] = the upslope contributing area for each cell (result of the ArcGIS “flowacc” and “resolution” functions), b [%] = slope, a_0 [m] = 21.1 m (the standard USLE plot length), and b_0 [%] = 9% (the standard USLE plot slope). The parameter μ is calculated as a function of β , which is the ratio of rill to interrill erosion (Miller et al. 2003; Foster et al. 2003):

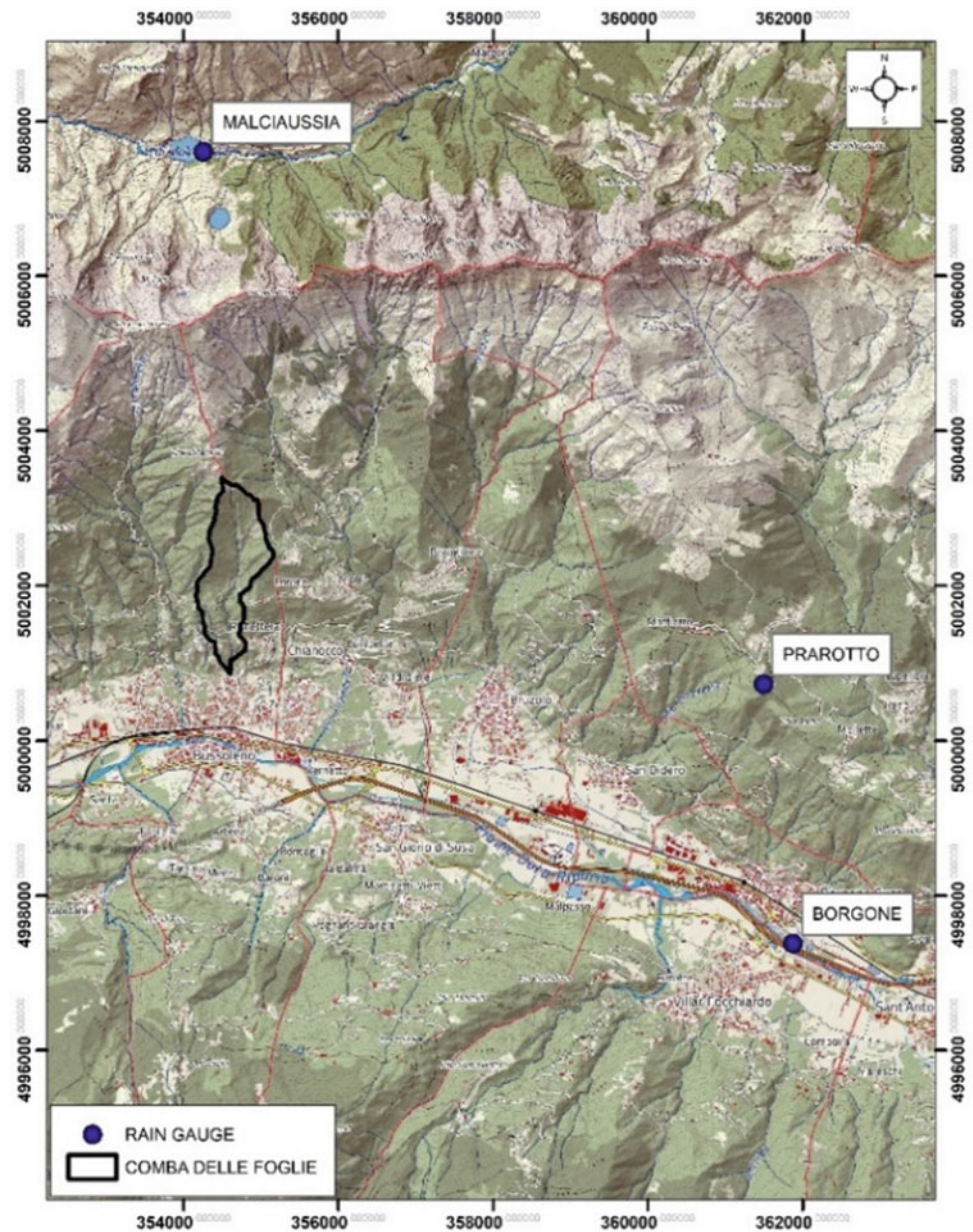
$$\mu = \beta / ((1 + \beta)) \quad (12)$$

Based on literature, β can be set equal to 0.5 for unburned areas and equal to 1 for burned areas with high severity. The parameter η is considered equal to 1.2 following Terranova et al. (2009) and Coschignano et al. (2020). The cell values in a buffer of 10 m around the stream network has been excluded from the calculation since the RUSLE model does not provide estimates for streamflow erosion. For them, a default value of 0 has been assigned.

Model implementation

Pre-fire monthly mean soil loss (A_{pre}) and erodibility index (EI_{pre}) were calculated based on the previous equations on a 5 m resolution raster grid based on DTM cells position.

Fig. 2 Location of the three rain gauges of Prarotto, Borgone and Malciaussia with respect to the Comba delle Foglie watershed position



377 Then the spatially weighted average of A_{w_pre} was calculated
378 over the entire watershed surface.

379 Finally, the value of the monthly sediment loss (SL_{pre})
380 [$Mg\ y^{-1}$] for the watershed was calculated multiplying the
381 value of A_{w_pre} times the watershed area. Post-fire condition
382 was modeled by calculating mean soil loss per month (A_{post})
383 and erodibility index (EI_{post}) following Eqs. (3) and (4). The
384 single factors of the RUSLE model were adjusted as a
385 function of fire severity (unburned, low, moderate or high)
386 following with some modifications the procedures described
387 in Terranova et al. (2009) and Lanorte et al. (2019). The
388 metrics used in this work are given in Table 5. For both
389 scenarios (pre- vs post-fire), A and EI raster cell values have

been subsequently averaged for each watershed giving
390 A_{w_post} and SL_{post} value.

392 4 Results

393
394 The fire severity class distribution over the watershed
395 (Fig. 3) highlight a predominancy (77.10%) of moderate fire
396 severity, while unburned/low and high severity cover the
397 21.98%, and 0.92% of the watershed area, respectively.
398 Given the fact that the area experienced another fire in 2003,
399 the burn severity map may underestimate the 2017 situation,
400 even if a relativized index such as RdNBR has been used.

Table 3 RUSLE cover factor proposed for each land cover class (after Panagos et al. 2015b)

CLC class	Class name	C-factor values	CLC class	Class name	C-factor values
112	Discontinuous urban fabric	0	313	Mixed forest	0.0013
131	Mineral extraction sites	0	313b	Mixed forest < 20%	0.003
211	Non-irrigated arable land	0.23	3211	Natural grassland prevailingly without trees and shrubs	0.04
221	Vineyards	0.34	3212	Natural grassland with trees and shrubs	0.03
222	Fruit trees and berry plantations	0.1	322	Moors and heathland	0.055
231	Pastures	0.09	322b	Moors and heathland	0.055
242	Complex cultivation patterns	0.147	324	Transitional woodland-shrub	0.024
243	Land principally used for agriculture, with significant areas of natural vegetation	0.124	332	Bare rocks	0
311	Broad-leaved forest	0.0013	333	Sparsely vegetated areas	0.25
311b	Broad-leaved forest < 20%	0.003	0	Bare Soil	1
312	Coniferous forest	0.0013			
312b	Coniferous forest < 20%	0.003			

Table 4 Land cover classes areal distribution over the Comba delle Foglie watershed

Land principally used for agriculture	Broad-leaved forest	Mixed forest	Transitional woodland-shrub	Broad-leaved forest < 20%	Mixed forest < 20%	Natural grassland with trees and shrubs
%	%	%	%	%	%	%
5.5	24.5	38.2	4.2	0.6	26.1	0.9

Table 5 Adjusted cover factors (C), erodibility factors (K) and β value (used for LS factor calculation) (β) for different fire severity classes

Burn Severity class	RUSLE parameters		
	C	K	β
Unburned/Low	C_{pre}	K_{pre}	0.5
Moderate	$C_{pre} + 0.1$	$1.8 * K_{pre}$	1
High	$C_{pre} + 0.25$	$2 * K_{pre}$	1

401 Monthly R factors for each rain gauge from September
 402 2017 to August 2018 have been quantified by calculating the
 403 summation of the parameter EI_{30} of every single erosive
 404 event for each considered month. The R factor obtained for
 405 each station has been then averaged for assessing the rep-
 406 resentative rainfall erosive power at the watershed scale. For
 407 the Prarotto, Borgone and Malciaussia rain gauges 22, 24
 408 and 22 erosive events, respectively, have been identified. For
 409 the Prarotto rain gauge, the selected storms are characterized
 410 by a mean precipitation value of 30.94 mm, duration of
 411 23.23 h and EI_{30} of 95.99 MJ mm ha⁻¹ h⁻¹. For the Bor-
 412 gone rain gauge mean precipitation, duration and EI_{30} val-
 413 ues are 27.67 mm, 20.19 h and 73.06 MJ mm ha⁻¹ h⁻¹. At
 414 the Malciaussia station, mean value recorded are 29.20 mm,
 415 16.02 h and 55.40 MJ mm ha⁻¹ h⁻¹, for precipitation,

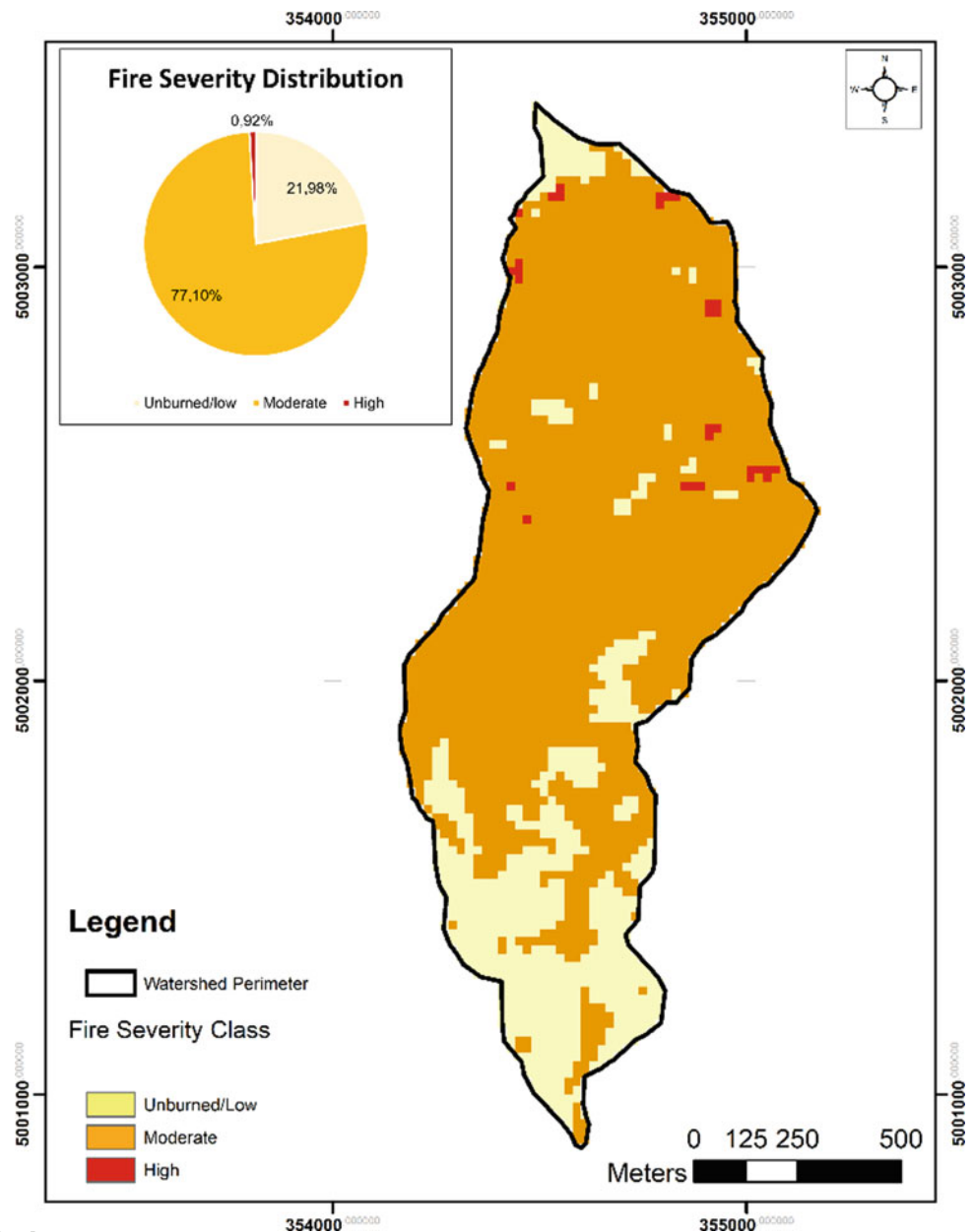
416 duration and EI_{30} . The maximum values of R factor are
 417 reached in May, April and March 2018, and are, on the
 418 contrary, equal to zero for September and October 2017.

419 R factor distribution over time is consistent with Pied-
 420 mont meteorological data (Arpa Piemonte 2018a, b, 2019),
 421 reporting an extremely dry end of 2017 and very wet month
 422 of January, April and May 2018. In fact, erosive events
 423 registered in these months represents approximatively the
 424 75% of the entire annual R factor, and in particular the
 425 month of May reaching almost the 40%. Erodi-
 426 bility K factor representative of the pre-fire condition has been determined
 427 based on soil textural data collected during the field surveys.

428 The pre-fire K values have been calculated following Eqs.
 429 (9) and (10). The post-fire adjusted K values have been then
 430 calculated by applying the correction procedure described in
 431 Table 5. Pre-fire and post-fire K values are reported in Fig. 4
 432 (a, b). Pre-fire c factor (Fig. 4c) has been calculated following
 433 the procedure described above, by using the values reported
 434 in Table 3; post-fire c factor (Fig. 4d) has been then calcu-
 435 lated as given in Table 5. Pre-fire LS factor has been calcu-
 436 lated through Eqs. (11) and (12), while post-fire LS values
 437 have been calculated through Eq. 12 and Table 5. Results are
 438 reported in Fig. 4e, f. P value has been set equal to 1.

439 Erodi-
 440 bility index values for the pre-fire and post-fire sit-
 441 uation (Table 6) has been calculated following Eq. (5), and

Fig. 3 Fire severity classes distribution for the Comba delle Foglie catchment



441 finally monthly mean soil loss A [$\text{Mg ha}^{-1} \text{m}^{-1}$] and averaged 442
443 monthly sediment loss SL [Mg m^{-1}] for the entire watershed have been computed for both the burned and 444
445 unburned condition. The post-fire mean erodibility index is more than one order of magnitude higher than the pre-fire 446
447 one, having a pre-fire value of $4.63\text{E-}04 \text{ Mg MJ}^{-1} \text{ mm}^{-1} \text{ h}$ and a post fire value of $1.21\text{E-}02 \text{ Mg MJ}^{-1} \text{ mm}^{-1} \text{ h}$. Also, 448
449 the maximum values show a rise of about the same order.

450 Monthly mean soil loss A [$\text{Mg ha}^{-1} \text{m}^{-1}$] and averaged 451
452 monthly sediment loss SL [Mg m^{-1}] comparison for the pre- and post-fire conditions (Fig. 5, Table 7) results in a post-fire 453
454 increase of both the indicators of more than 20 times with respect to pre-fire. Maximum pre-fire values occur in May,

454 being $0.307 \text{ Mg ha}^{-1} \text{m}^{-1}$ and 39.86 Mg m^{-1} for monthly 455
456 mean soil loss and monthly sediment loss, respectively; for the post-fire, these parameters reach values of 8.066 Mg 457
458 $\text{ha}^{-1} \text{m}^{-1}$ and $1050.400 \text{ Mg m}^{-1}$, respectively.

5 Discussion

460 The sediment erosion has been assessed for the Comba delle 461
462 Foglie watershed by implementing the RUSLE model at a monthly scale, including model inputs of a detailed erodi- 463
464 bility map, the forestry/land cover map, the LS factor map derived from GIS elaboration and a R factor value calculated

Fig. 4 RUSLE factors distribution over the catchment: pre-fire erodibility factor **a**, post-fire erodibility **b**, pre-fire cover factor **c**, post-fire cover factor **d**, pre-fire LS factor **e** and post-fire LS factor **f**

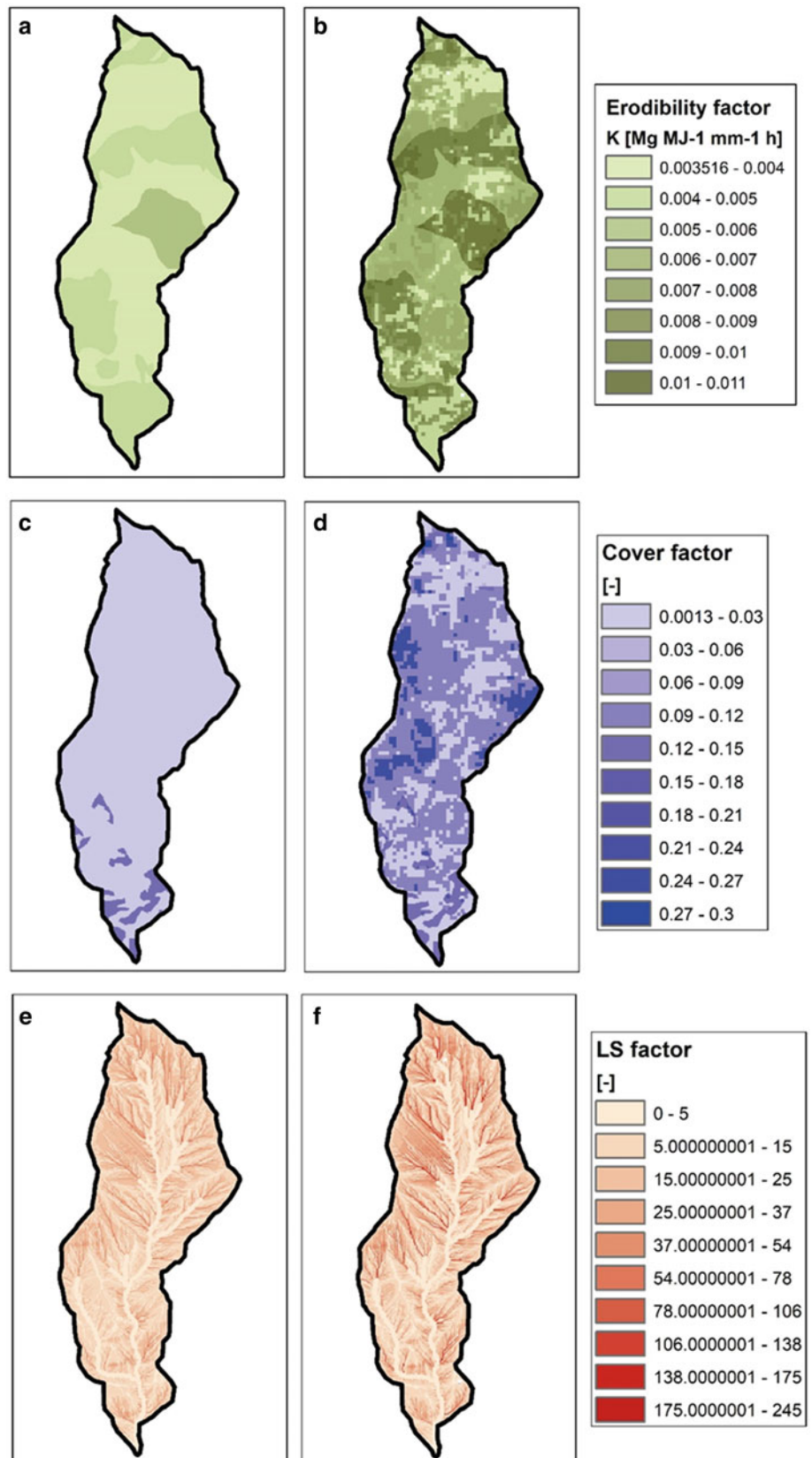


Table 6 Post-fire versus pre-fire erodibility index values over the Comba delle Foglie watershed

EI [$\text{Mg MJ}^{-1} \text{mm}^{-1} \text{h}$]	Pre-fire	Post-fire
MIN	0.00E + 00	0.00E + 00
MAX	2.83E - 02	3.54E - 01
MEAN	4.63E - 04	1.22E - 02
STD	1.65E - 03	2.16E - 02

by retrieving the erosive power of every significant rainfall event. Monthly mean soil loss [$\text{Mg ha}^{-1} \text{m}^{-1}$] and averaged monthly sediment loss [Mg m^{-1}] are the result of the remarkably R values recorded in the months of January, April and May; these three months in fact contribute for about 75% to the annual erosion recorded in the watershed.

Comparing the calculated R factors to average monthly R factor by Ballabio et al (2017) (Fig. 6) is evident a concentration of the erosive events in the post-fire time window, while the precipitations remained well below the average values from September to December 2017, barely reaching the 6% of the cumulated average value. The months of January, April and May show values eleven, eight and four times greater, respectively, than the long time series data. The RUSLE model estimates a SL of approximately 2430 Mg from the extinction of the fire to June (included), when the most significant event occurred. To validate this result, the only available information is related to the characterization of the 7 June event: in that case, the maximum deposit thickness of the debris-flow reconstructed via photogrammetric modelling was approximately 2 m and the invasion area covered about 26,000 m^2 . The total mobilized volume for only the coarser fraction of the deposit, was about 4300 m^3 , of which about 1500 m^3 consisting of materials entrained just at the fan apex. The volume of the coarser sediments coming from the watershed was estimated to be 1300 m^3 . By applying a simple rule of thumb, considering a bulk density of 1500 kg/m^3 , the 7 June flow mass can be estimated in 1950 Mg. Considering the fact that other four minor events (one debris/mud flow in April and three floods in May) happened before the 7 June, it is reasonable to presume that the remnant part of the total sediment loss estimated by the model could be related to those events. Some non-negligible aspects undermine the model robustness and accuracy: in fact, the 7 June event volume estimated via photogrammetrical modeling contrast with the one suggested by Arpa Piemonte (2018b), which after expeditive surveys estimates the total event volume to be about 20,000 m^3 . Another aspect which should be taken into account when dealing with the model validation is the remarkable erosion exerted by the debris-flows along all their paths, which may have increased their volumes considerably. The results of the model are not suitable to predict

streamflow erosion, so when the estimated value is compared to the available surveyed data, this aspect may also increase the uncertainty. Finally, the current model does not take into account the ash and combustion residues which, for sure, contribute to the overall sediment availability to be entrained. Ash and combustion residues are expected to constitute a large part of the removable material especially immediately after the fire, and that they will then be gradually washed away by the runoff as the rainy events occur. Despite all the model limitations and the uncertainties related to its validation, the presented procedure can be considered a reasonable estimator of the amount of material ready to be eroded during the rainstorm events and conveyed in the riverbeds. In fact, it is backed up by ground evidence, the assumption that the considerable amount of sediment mobilized from the date of the fire have been progressively delivered towards the bottom of the slopes and inside the stream network on the repeated rainfalls. In occasion of some smaller mud-flows and hyper-concentrated flows have originated. Then, when the progressive increase of sediments reached a critical threshold in conjunction with a rainy event of a sustained intensity, the most destructive debris-flow on 7 June occurred. During the field inspections prior to 7 June a considerable amount of sediments and combustion residues had been observed inside the channels, especially in the terminal part of the watershed and at the apex of the fan. The investigations carried out following the event revealed evident traces of areal and channeled erosion, starting from the upper part of the slopes and into the lower-order channels. It is clear how all this mass of sediments, both coming from open slopes and being deposited in the drainage network, has constituted the load of the debris-flow during its transit, simultaneously increasing its energy.

6 Conclusions

The Piedmont region, and in particular the western Italian Alps, experienced an unusually severe wildfire season in 2017. The fires occurred in the late autumn and, after a snowy winter, were followed by spring rains. In particular, some of the catchments burned in the Susa Valley wildfire were interested in May and June 2018 by debris/mud-flows and flood type events. The major debris-flow happened at the outlet of Comba delle Foglie and struck the Bussoleno municipality. Based on field evidence, it was found that the flows mobilized materials and sediments, which were eroded from the burned hillslopes and subsequently deposited in the channels. This is consistent with the literature which reported the main cause of the post-fire debris-flows to be the generation of increased erosion due to excess runoff rather than a discrete landslide failure. On the back of these findings, a modified version of the RUSLE model was applied in

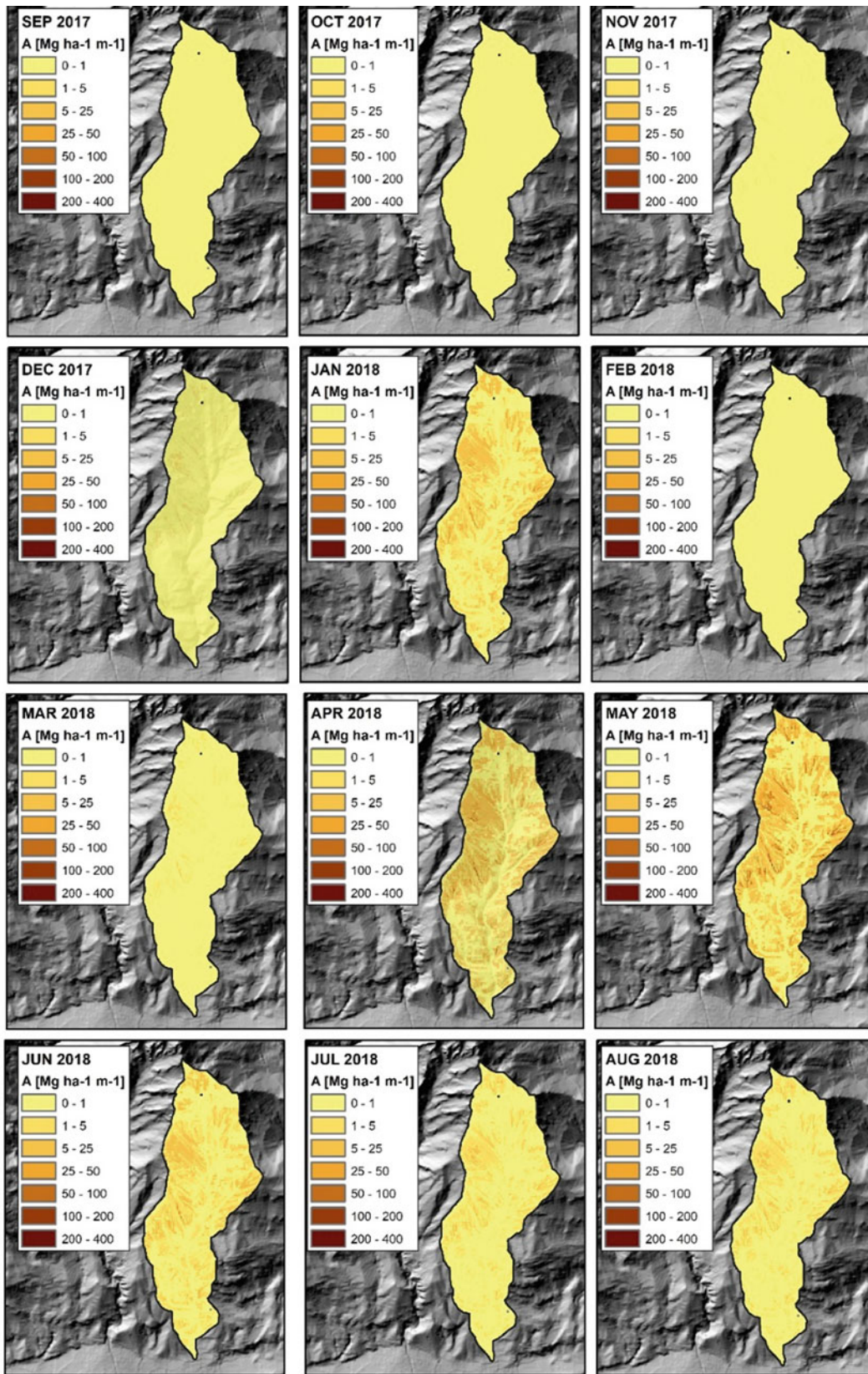
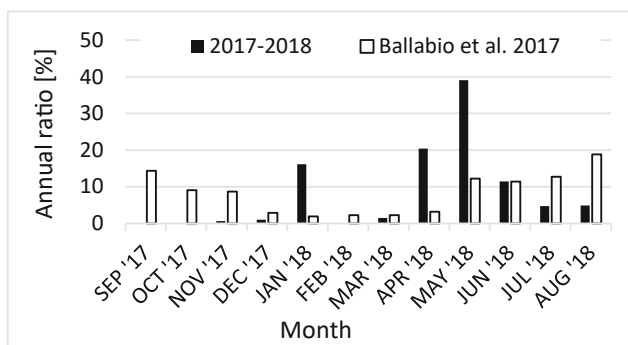


Fig. 5 Monthly mean soil loss

Table 7 Spatially averaged mean soil loss (A) and averaged monthly sediment loss (SL) comparison for the burned and unburned situation

Month	Burned		Unburned	
	A	SL	A	SL
	[Mg/ha*m]	[Mg/m]	[Mg/ha*m]	[Mg/m]
9–17	0.000	0.00	0.000	0.00
10–17	0.000	0.00	0.000	0.00
11–17	0.133	17.32	0.005	0.66
12–17	0.208	27.07	0.008	1.03
1–18	3.342	434.36	0.127	16.48
2–18	0.014	1.82	0.001	0.07
3–18	0.310	40.28	0.012	1.53
4–18	4.223	548.87	0.160	20.83
5–18	8.081	1050.28	0.307	39.86
6–18	2.371	308.14	0.090	11.69
7–18	0.981	127.55	0.037	4.84
8–18	1.014	131.75	0.038	5.00
TOT	20.677	2687.45	0.785	101.98

**Fig. 6** Comparison between calculated and long term inter annual R-factor (Ballabio et al. 2017)

it does not incorporate the eroded volume of ash and combustion residues. Some uncertainties are then linked to the fact that the estimates regarding the actual volumes of the flows are limited to a single case (the major one, 7th June) and also do not agree with each other. Despite these uncertainties, the proposed procedure can be considered a reasonable estimator of the amount of material ready to be eroded, especially if it is used to compare different catchments in a relative way; in this case, it can provide useful guidance to rank the post-fire debris-flow susceptibility and to establish intervention priorities. It can be applied everywhere on the regional territory because the model make use on open-source spatialized data and thanks to its structure, it can be easily implemented into a GIS for thematic map production.

the area of Comba delle Foglie to quantify the erosive processes on a monthly scale. The results of its application, incorporating high resolution rainfall series and data deriving from field surveys, made it possible to reproduce and highlight the marked increase in erosion rates, quantified by expressing both the EI (erodibility index), the A (monthly soil loss) and the SL (monthly sediment loss) rise. In particular, overall A and SL increased more than twenty times in the post-fire scenario, the months of April, May and June representing the larger share of the total quantities. This is a consequence of the noticeable increase of t EI, which for the post-fire scenario is more than one order of magnitude higher than the pre-fire one. The intrinsic uncertainties of the model are related to the fact that it does not consider the stream-flow erosion in the channels, it does not account for the material eroded by the debris-flow during its passage and

Acknowledgements This study is conducted within the ICL IPL project No. 4938. Many thanks to Arpa Piemonte for rainfall data. Field survey were conducted in the framework of the Institutional Technical Table on Wildfire Emergency of the Piedmont Region.

References

- Arndt N, Vacik H, Koch V, Arpaci A, Gossow H (2013) Modeling human-caused forest fire ignition for assessing forest fire danger in Austria. *Iforest* 6:315–325
- Arpa Piemonte (2017) Rapporto tecnico sulla qualità dell'aria e sulle attività dell'agenzia a supporto dell'emergenza per gli incendi boschivi in Piemonte nel mese di ottobre 2017
- Arpa Piemonte (2018a) Rapporto evento del 07/06/2018, Colata detritica nel comune di Bussoleno
- Arpa Piemonte (2018b) Il Clima in Piemonte 2017. Available online at <https://www.arpa.piemonte.it>

559
560
561
562
563
564
565
566
567
568
569
570
571
572
573
574575
576
577
578
579
580
581
582
583
584
585
586
587
588
589
590
591
592
593
594
595
596
597
598
599
600
601
602
603
604
605



- 606 Arpa Piemonte (2019) Il Clima in Piemonte 2018. Available online at
607 <https://www.arpa.piemonte.it>
- 608 Ascoli D, Valsecchi C, Bovio G and Conedera M (2011) Wildfires and
609 beech forests of Southern Alps during the summer 2003 climate
610 anomaly: fire effects and post-fire management. The 5th international
611 wildland fire conference, Sun City, South Africa, 9–13 May 2011
- 612 Ballabio C, Borrelli P, Spinoni J, Meusburger K, Michaelides S,
613 Beguería S, Klik A, Petan S, Janecek M, Olsen P, Aalto J,
614 Lakatos M, Rymaszewicz A, Dumitrescu A, Tadić MP, Nazzareno D,
615 Kostalova J, Rousseva S, Banasik KL, Alewell C, Panagos P (2017)
616 Mapping monthly rainfall erosivity in Europe. *Sci Total Environ*
617 579:1298–1315
- 618 Barbero R, Curt T, Ganteaume A, Maillé E, Jappiot M, Bellet A (2019)
619 Simulating the effects of weather and climate on large wildfires in
620 France. *Nat Hazards Earth Syst Sci* 19:441–454
- 621 Bo M, Mercalli L, Pognant F, Cat Berro D, Clerico M (2020) Urban air
622 pollution, climate change and wildfires: the case study of an
623 extended forest fire episode in northern Italy favoured by drought
624 and warm weather conditions. *Energy Rep* 6:781–786
- 625 Brown LC, Foster GR (1987) Storm erosivity using idealized intensity
626 distributions. *Trans Am Soc Agric Eng* 30:379–386
- 627 Cadoppi P, Giardino M, Perrone G, Tallone SD (2007) Litho-structural
628 control, morphotectonics, and deep-seated gravitational deforma-
629 tions in the evolution of Alpine relief: a case study in the lower Susa
630 Valley (Italian Western Alps). *Quatern Int* 171:143–159
- 631 Carabella C, Miccadei E, Paglia G, Sciarra N (2019) Post-wildfire
632 landslide hazard assessment: the case of the 2017 montagna del
633 morrone fire (central apennines, Italy). *Geosciences* 9:175
- 634 Carraro F, Cadoppi P, Baggio P, Bellino L, Castelletto M, Giraud V,
635 Mensio L (2002) Foglio 154 – Susa – Carta Geologica d’Italia, scala
636 1:50.000. Carta Geol—Serv Geol D’Italia Coord CARRARO F 126
- 637 Coschignano G, Nicolaci A, Ferrari E, Cruscomagno F and Iovino F
638 (2019) Evaluation of hydrological and erosive effects at the basin
639 scale in relation to the severity of forest fires. *iForest* 12:427–434
- 640 De Graff JV (2014) Improvement in quantifying debris flow risk for
641 post-wildfire emergency response. *Geoenviro Disasters* 1:5
- 642 Depountis N, Michalopoulou M, Kavoura K, Nikolakopoulos K,
643 Sabatakakis N (2020) Estimating soil erosion rate changes in areas
644 affected by wildfires. *ISPRS Int J Geo-Inf* 9:562
- 645 Dupire S, Curt T, Bigot S, Fréjaville T (2019) Vulnerability of forest
646 ecosystems to fire in the French Alps. *Eur J For Res* 138:813–830
- 647 Eftimiou N, Psomiadis E, Panagos P (2020) Fire severity and soil
648 erosion susceptibility mapping using multi-temporal earth observa-
649 tion data: the case of Mati fatal wildfire in Eastern Attica, Greece.
650 *Catena* 187(2020):104320
- 651 Esposito G, Esposito E, Matano F, Molisso F, Sacchi M, Porfido S
652 (2013) Effects of a wildfire on rocks and soils in the Sarno
653 Mountains, Campania, Southern Apennines. *Rend Online Soc Geol*
654 *Ital* 24:119–121
- 655 Esposito G, Matano F, Molisso F, Ruoppolo G, Di Benedetto A,
656 Sacchi M (2017) Post-fire erosion response in a watershed mantled
657 by volcanoclastic deposits, Sarno Mountains, Southern Italy.
658 *CATENA* 152:227–241
- 659 Esposito G, Parodi A, Lagasio M, Masi R, Nanni G, Russo F, Alfano S,
660 Giannatiempo G (2019) Characterizing consecutive flooding events
661 after the 2017 Mt. Salto Wildfires (Southern Italy): Hazard and
662 emergency management implications. *Water* 11:2663
- 663 Esteves TCJ, Kirkby MJ, Shakesby RA, Ferreira AJD, Soares J,
664 Irvine B, Ferreira CSS, Coehlo COA, Bento CPM, Carreira M
665 (2012) Mitigating land degradation caused by wildfire: application
666 of the PESERA model to fire-affected sites in central Portugal.
667 *Geoderma* 191:40–50
- 668 Fernandez C, Vega JA (2018) Evaluation of the RUSLE and disturbed
669 wepp erosion models for predicting soil loss in the first year after
670 wildfire in NW Spain. *Environ Res* 165:279–285
- Fernandez C, Vega JA, Vieira DCS (2010) Assessing soil erosion after
671 fire and rehabilitation treatments in NW Spain: performance of
672 RUSLE and revised Morgan–Morgan–Finney models. *Land Degrad*
673 *Dev* 21:58–67
- Foster GR, Toy TJ, Renard KG (2003) Comparison of the USLE,
674 RUSLE1.06c, and RUSLE2 for application to highly disturbed
675 lands. Proceedings of the first interagency conference on research in
676 the watersheds. USDA—Agricultural Research Service, Washing-
677 ton, DC, pp 154–160
- 678 Gasco I, Gattiglio M, Borghi A (2011) Lithostratigraphic setting and
679 P-T metamorphic evolution for the Dora Maira Massif along the
680 Piedmont Zone boundary (middle Susa Valley, NW Alps). *Int J*
681 *Earth Sci* 100:1065–1085
- Horton RE (1932) Drainage-basin characteristics. *EOS Trans Am*
682 *Geophys Union* 13:350–361
- IPCC (2014a) Synthesis report. In: Core Writing Team, Pachauri RK,
683 Meyer LA (eds) Climate change 2014. Contribution of working
684 groups I, II and III to the fifth assessment report of the
685 intergovernmental panel on climate change. IPCC, Geneva
- IPCC (2014b) Climate change 2014: impacts adaptation and vulner-
686 ability. Part A. Global and sectoral aspects. In: Field CB, Barros VR,
687 Dokken DJ, Mach KJ, and others (eds) Contribution of working
688 group II to the fifth assessment report of the intergovernmental
689 panel on climate change. Cambridge University Press, Cambridge
- Key CH, Benson NC (2006) Landscape assessment (LA): sampling and
690 analysis methods. In: Lutes D, Keane RE, Caratti JF, Key CH,
691 Benson NC, Sutherland S, Gangi L (eds) Firemon: fire effects
692 monitoring and inventory system. RMRS-GTR-164; Rocky Moun-
693 tain Research Station, US Department of Agriculture, Forest
694 Service: Fort Collins, CO, USA, 2006; pp LA-1–LA-51
- Kirpich ZP (1940) Time of concentration of small agricultural
695 watersheds. *Civ Eng* 10(6):362
- Lanorte A, Cillis G, Calamita G, Nolè G, Pilogallo A, Tucci B, Santis F
696 (2019) Integrated approach of RUSLE, GIS and ESA Sentinel-2
697 satellite data for post-fire soil erosion assessment in Basilicata
698 region (Southern Italy). *Geomat Nat Haz Risk* 10(1):1563–1595
- Mantero G, Morresi D, Marzano R, Motta R, Mladenoff DJ, Gar-
699 barino M (2020) The influence of land abandonment on forest
700 disturbance regimes: a global review. *Landscape Ecol* 35:2723–
701 2744. <https://doi.org/10.1007/s10980-020-01147-w>
- Maringer J, Ascoli D, Dorren L, Bebi P, Conedera M (2016) Temporal
702 trends in the protective capacity of burnt beech forests (*Fagus*
703 *sylvatica* L.) against rockfall. *Eur J For Res* 135(4):657–673
- Melton MA (1965) The geomorphic and paleoclimatic significance of
704 alluvial deposits in Southern Arizona. *J Geol* 73:1–38
- Miller JD, Thode AE (2007) Quantifying burn severity in a heteroge-
705 neous landscape with a relative version of the delta normalized burn
706 ratio (dNBR). *Remote Sens Environ* 109:66–80
- Miller JD, Nyhan JW, Yool SR (2003) Modeling potential erosion due
707 to the Cerro Grande fire with a GIS-based implementation of the
708 revised universal soil loss equation. *Int J Wildland Fire* 12:85–100
- Miller VCA (1953) Quantitative geomorphic study of drainage basin
709 characteristics in the Clinch Mountain area Virginia and tennessee.
710 Columbia University Technology Report No. 3, Contract N6 ONR,
711 pp 271–30
- Mitasova H, Hofierka J, Zlocha M, Iverson LR (1996) Modeling
712 topographic potential for erosion and deposition using GIS. *Int J*
713 *Geogr Inf Sci* 10(5):629–641
- Moody JA, Martin PA (2001) Initial hydrologic and geomorphic
714 response following a wildfire in the Colorado front range. *Earth Surf*
715 *Proc Land* 26:1049–1070
- Moreira F, Viedma O, Arianoutsou M, Curt T, Koutsias N, Rigolot E,
716 Barbati A, Corona P, Vaz P, Xanthopoulos G, Mouillot F, Bilgili E
717 (2011) Landscape - wildfire interactions in southern Europe: impli-
718 cations for landscape management. *J Environ Manage* 92:2389–2402



736 Morresi D, Marzano R, Lingua E, Motta R, Garbarino M (2022) 775
737 Mapping burn severity in the western Italian Alps through 776
738 phenologically coherent reflectance composites derived from 777
739 Sentinel-2 imagery. *Remote Sens Environ* 269:112800 778
740 Panagos P, Ballabio C, Borrelli P, Meusburger K, Klik A, Rousseva S, 779
741 Tadic MP, Michaelides S, Hrabalíková M, Olsen P, Aalto J, 780
742 Lakatos M, Rymaszewicz A, Dumitrescu A, Begueria S, Alewell C 781
743 (2015a) Rainfall erosivity in Europe. *Sci Total Environ* 511:801– 782
744 814 783
745 Panagos P, Borrelli P, Meusburger K, Alewell C, Lugato E, Mon- 784
746 tanarella L (2015b) Estimating the soil erosion cover-management 785
747 factor at the European scale. *Land Use Policy* 48(2015):38–50 786
748 Parise M, Cannon SH (2008) The effects of wildfires on erosion and 787
749 debris-flow generation in Mediterranean climatic areas: a first 788
750 database. *Proceedings of 1st world landslide forum. Tokyo, Japan,* 789
751 *pp 465–468* 790
752 Parise M, Cannon SH (2012) Wildfire impacts on the processes that 791
753 generate debris flows in Burned Watersheds: *Natural Hazards, vol* 792
754 *61* 793
755 Parks SA, Dillon GK, Miller C (2014) A new metric for quantifying 794
756 burn severity: the relativized burn ratio. *Remote Sens* 6:1827–1844 795
757 Renard KG, Foster GR, Weesies GA, McCool DK, Yoder DC (1997) 796
758 Predicting soil erosion by water: a guide to conservation planning 797
759 with the revised universal soil loss equation (RUSLE) (*Agricultural* 798
760 *handbook 703*). US Department of Agriculture, Washington, DC, 799
761 *p 404* 800
762 Rulli MC, Offeddu L, Santini M (2013) Modeling post-fire water 801
763 erosion mitigation strategies. *Hydrol Earth Syst Sci* 17:2323–2337 802
764 Schumm SA (1956) Evolution of drainage systems and slopes in 803
765 badlands at Perth Amboy. *New Jersey, Geol Soc Am Bull* 67:597– 804
766 646 805
767 Sheridan GJ, Lane PN, Smith H, Nyman P (2009) A rapid risk 806
768 assessment procedure for post-fire hydrologic hazards; 2009/10 fire 807
769 season. Technical report produced for the department of sustain- 808
770 ability and environment. The Department of Forest and Ecosystem 809
771 Science, The University of Melbourne, Australia, *p 19*. ISBN 810
772 9780734041470 811
773 Staley DM, Negri JA, Kean JW, Laber JL, Tillery AC, Youberg AM 812
774 (2017) Prediction of spatially explicit rainfall intensity–duration 813
814 thresholds for post-fire debris-flow generation in the Western United 815
816 States. *Geomorphology* 278:149–162 817
818 Staley DM, Negri JA, Kean JW, Tillery AC, Youberg AM (2016) 819
820 Updated logistic regression equations for the calculation of post-fire 820
821 debris-flow likelihood in the western United States: U.S. Geological 821
822 Survey Open-File Report 2016–1106, *p 13* 822
823 Strahler AN (1964) Quantitative geomorphology of drainage basin and 823
824 channel networks. *Handbook of applied hydrology* 824
825 Tang H, McGuire LA, Rengers FK, Kean JW, Staley DM, Smith JB 825
826 (2019) Evolution of debris-flow initiation mechanisms and sediment 826
827 sources during a sequence of postwildfire rainstorms. *J Geophys* 827
828 *Res Earth Surf* 124:1572–1595 828
829 Terranova O, Antronico L, Coscarelli R, Iaquina P (2009) Soil erosion 829
830 risk scenarios in the Mediterranean environment using RUSLE and 830
831 GIS: an application model for Calabria (southern Italy). *Geomor-* 831
832 *phology* 112(2009):228–245 832
833 Tiranti D, Moscariello A, Giudici I, Rabuffetti D, Cremonini R, 833
834 Campana V, Bosco F, Giardino M (2006) Post-fire rainfall events 834
835 influence on debris-flows trigger mechanisms, evolution and 835
836 sedimentary processes: the Rio Casella case study in the 836
837 North-western Italian Alps. *Geophys Res Abstr* 8:03479 837
838 USDA (2014) United States department of agriculture. Rainfall Intensity 838
839 Summarization Tool (RIST). Accessed from, [http://www.ars.usda](http://www.ars.usda.gov) 839
840 [.gov](http://www.ars.usda.gov) 840
841 Vacha D, Mandrone G, Garbarino M, Morresi D (2021) First 841
842 consideration about post 2017 wildfire erosion response and debris 842
843 flow in Susa Valley (NW Italy). In: Tiwari B, Sassa K, 843
844 Bobrowsky PT, Takara K (eds) *Understanding and reducing* 844
845 *landslide disaster risk. WLF 2020. ICL contribution to landslide* 845
846 *disaster risk reduction*. Springer, Cham 846
847 Wastl C, Schunk C, Leuchner M, Pezzatti B, Menzel A (2012) Recent 847
848 climate change: long-term trends in meteorological forest fire 848
849 danger in the Alps. *Agric for Meteorol* 162–163:1–13 849
850 Wischmeier WH, Smith DD (1978) Predicting rainfall erosion losses: a 850
851 guide to conservation planning. *Agriculture Handbook no. 537,* 851
852 *USDA, Washington DC, USA, pp 13–27* 852
853 Zumbrennen T, Bugmann H, Conedera M, Bürgi M (2009) Linking 853
854 forest fire regimes and climate—a historical analysis in a dry inner 854
855 Alpine valley. *Ecosystems* 12:73–86 855

Author Proof

815
816 **Open Access** This chapter is licensed under the terms of the Creative Commons Attribution 4.0 International License (<http://creativecommons.org/licenses/by/4.0/>), which permits use, sharing, adaptation, distribution and reproduction in any medium or format, as long as you give appropriate credit to the original author(s) and the source, provide a link to the Creative Commons license and indicate if changes were made.
818
819 The images or other third party material in this chapter are included in the chapter’s Creative Commons license, unless indicated otherwise in a credit line to the material. If material is not included in the chapter’s Creative Commons license and your intended use is not permitted by statutory regulation or exceeds the permitted use, you will need to obtain permission directly from the copyright holder.
822
823



Author Query Form

825

826
828
829
827

Book ID : 525824_1_En

Chapter No : 6

830
831

Please ensure you fill out your response to the queries raised below and return this form along with your corrections.

832
833
834
835

Dear Author,

During the process of typesetting your chapter, the following queries have arisen. Please check your typeset proof carefully against the queries listed below and mark the necessary changes either directly on the proof/online grid or in the 'Author's response' area provided below

840

839

843
844

846

Query Refs.	Details Required	Author's Response
AQ1	References 'Dupire et al. (2019), Thang et al. (2019), Key and Benson (2005)' are cited in the text but not provided in the reference list. Please provide the respective references in the list or delete these citations.	

UNCORRECTED PROOF

Author Proof